energies

MDPI

Article

Battery Fault Diagnosis Method Based on Online Least Squares Support Vector Machine

Tongrui Zhang [1,2,*], Ran Li [3] and Yongqin Zhou [3]

[1] Houston International Institute, Dalian Maritime University, Dalian 116026, China
[2] Cullen College of Engineering, The University of Houston, Houston, TX 77204, USA
[3] Engineering Research Center of Automotive Electronics Drive Control and System Integration, Ministry of Education, Harbin University of Science and Technology, Harbin 150080, China; liran@hrbust.edu.cn (R.L.)
* Correspondence: ztr020917@dlmu.edu.cn

Abstract: Battery fault diagnosis technology is crucial for the reliable functioning of battery systems. This research introduces an online least squares support vector machine method tailored for battery fault diagnosis. After examining battery fault types and gathering relevant data, this method creates a diagnostic model, effectively addressing small and sporadic fault data that is inadequately handled by conventional support vector machines. Recognizing that certain battery malfunctions evolve over time and are multifaceted, confidence intervals have been integrated into the diagnostic models, enhancing accuracy. Upon testing this model using empirical data, it demonstrated rapid diagnostic capabilities and outperformed other algorithms in identifying progressive faults, ensuring precise fault identification, minimizing false alarms, and bolstering battery system safety.

Keywords: lithium battery; online least squares support vector machine; fault diagnosis

check for updates

Citation: Zhang, T.; Li, R.; Zhou, Y. Battery Fault Diagnosis Method Based on Online Least Squares Support Vector Machine. *Energies* **2023**, *16*, 7273. https://doi.org/10.3390/en16217273

Academic Editor: Quanqing Yu

Received: 4 September 2023
Revised: 14 October 2023
Accepted: 23 October 2023
Published: 26 October 2023

Copyright: © 2023 by the authors. Licensee MDPI, Basel, Switzerland. This article is an open access article distributed under the terms and conditions of the Creative Commons Attribution (CC BY) license (https://creativecommons.org/licenses/by/4.0/).

1. Introduction

Lithium-ion batteries have emerged as preferred energy storage solutions owing to their efficient and stable charge/discharge attributes [1–4]. However, they present a complex chemical system where energy storage and transfer involve intricate chemical reactions, posing potential combustion or explosive risks. Battery malfunctions can trigger cascading failures, potentially incapacitating the entire system [5]. As such, real-time fault diagnosis and understanding the underpinnings of these batteries are paramount for system reliability and safety [6].

Battery faults can be broadly classified into external categories, such as thermal [7], circuit [8], and sensor faults [9], as well as internal long-term failures, such as overcharging, discharge, and aging [10]. The external characteristics of long-term battery failures are not obvious. Early battery fault diagnosis relies on battery models, which often involve estimating the battery state to obtain more accurate estimates of the battery's SOH [11,12] and SOC [13]. However, with the upgrading of computer computing power, data-driven battery fault diagnosis methods have received more attention [14]. Its advantage is that it does not rely on estimated data but only requires real-time voltage collection. Information such as the current and temperature can be used to diagnose battery faults.

Battery data exhibits nonlinearity and significant temporal variability due to operational fluctuations. Historically, expert diagnostic systems, notably fuzzy expert systems, have been employed to navigate these battery system intricacies. Structurally, fuzzy expert systems mirror traditional expert systems, encompassing components like input, output, knowledge base, inference engine, knowledge acquisition, and explanatory modules. Through rigorous training on abundant representative data, these systems can achieve commendable diagnostic accuracy [15]. Da-Wei Z et al. [16] leveraged expert system knowledge for diagnosing faults in electric vehicles. Wei M et al. [17] combined professional knowledge with observed fault patterns for battery fault classification and diagnosis. In

Li et al. [18], a blend of probability theory and signal detection focused on discerning lithium-ion battery states based on electrical attributes influenced by operational duty cycles. Qiang et al. [19] evaluated changes in the battery's open-circuit voltage, paired with capacity degradation, using a model-based strategy to predict the battery state. However, this method demands extensive measurement time for accuracy, limiting its efficacy for real-time monitoring.

Data-centric methods remain at the forefront of diagnostic strategies. As computational technology has advanced, sensor-based diagnosis techniques have gained prominence, attributed to their adaptability and promptness. Adaikkappan M et al. [20] and Wang Y et al. [21] employed support vector machine (SVM) algorithms to ascertain the state of health (SOH) of batteries and fault identification. Meanwhile, Yibin T et al. [22] integrated neural networks, fuzzy logic, and autoregressive moving average techniques to scrutinize the impedance spectroscopy (IS) for fault node pinpointing within power grids.

This study introduces a battery fault diagnosis approach anchored on an online least squares support vector machine (OLS-SVM). By probing the external data variations induced by battery malfunctions, the least squares SVM algorithm delineates fault data boundaries and incorporates the notion of confidence intervals, especially for the battery's gradual type faults. Such an approach enables a refined quantification of battery degradation. With a data-centric diagnostic approach, distinct batteries and their data can be accommodated without necessitating updates during operation. Employing OLS-SVM assures both diagnostic precision and swift fault detection. Key innovations of this study include:

(1) collecting effective data on battery failure characteristics through experiments on battery aging, overcharging, and discharge faults;
(2) by utilizing increment and decrement algorithms, the update process of LS-SVM is simplified, greatly reducing the update time of the fault diagnosis model;
(3) incorporating confidence assessment metrics refines the quantification of composite battery fault nature and severity;
(4) the OLS-SVM algorithm can utilize new data for updates, taking into account the contribution of various types of data, effectively maintaining the data richness of training data, and better improving the accuracy of battery fault diagnosis.

2. Algorithm Principle

2.1. LS-SVM Principle Model for Batteries

The least squares support vector machine (LS-SVM) is an improved version of the SVM, which transforms the inequality constraints of traditional SVMs into an equality-constrained problem. It utilizes the sum of squared errors as the empirical loss of the training set, reducing computational complexity and increasing computational speed and robustness, thereby providing an effective solution for nonlinear binary classification [23]. Moreover, LS-SVM algorithms can be combined with binary tree theory to achieve multiclass classification, greatly expanding its range of applications. Given the training sample set $\{(x_i, y_i) | x_i \in R^S, y_i \in R = [-1, +1], i = 1, 2, \cdots, n\}$, in which x_i represents a n-dimensional input vector and y_i represents the output data of the LS-SVM model. The battery data model is linearly inseparable, thus, requiring data samples to be mapped from low-dimensional space to high-dimensional space through a nonlinear function $\varphi(x)$. Consequently, when constructing the optimal classification hyperplane of an SVM model in the high-dimensional feature space, the algorithm no longer considers the low-dimensional space but uses the training sample set in the high-dimensional feature space for computation, requiring the construction of kernel functions and decision functions:

$$K(x_i, x_j) = \varphi(x_i) \cdot \varphi(x_j) \tag{1}$$

$$y = \omega^T \varphi(x) + b \tag{2}$$

In the equation, ω and b are the parameters of LS-SVM regression model, where ω represents the weight vector and b represents the bias value.

Based on the principle of structural risk minimization, the optimization conditions of an LS-SVM regression model with slack variables e_i added can be obtained as follows:

$$\begin{aligned} &\min J(\omega, e) = \tfrac{1}{2}\omega^T\omega + \tfrac{1}{2}\gamma\sum_{i=1}^{n} e_i^2 \\ &s.t. y_i = \omega^T\omega(x_i) + b + e_i, i = 1, 2, \cdots, n \end{aligned} \tag{3}$$

In the equation, γ is the penalty factor and e_i is the error. Introducing the Lagrange multiplier, Equation (2) can be transformed as follows:

$$L(\omega, b, e, \alpha) = \frac{1}{2}\|\omega\|^2 + \frac{\gamma}{2}\sum_{i=1}^{n} e_i^2 - \sum_{i=1}^{n} \alpha_i\left(\omega^T\varphi(x_i) + b + e_i - y_i\right) \tag{4}$$

In the equation, $\alpha = [\alpha_1, \alpha_2, \cdots, \alpha_n]^T$ is the Lagrange multiplier. The optimal values of b and α can be obtained by satisfying KKT conditions, transforming the optimization problem to solve a linear equation system as follows:

$$\begin{bmatrix} 0 & 1^T \\ 1 & \Omega + \gamma^{-1}E \end{bmatrix}\begin{bmatrix} b \\ \alpha \end{bmatrix} = \begin{bmatrix} 0 \\ y \end{bmatrix} \tag{5}$$

In the equation, $\Omega_{ij} = K(x_i, x_j)$ is kernel function.

The discriminant function of LS-SVM classification model can be represented as follows based on the above equation:

$$y(x) = \sum_{i=1}^{n} \alpha_i K(x_i, x) + b \tag{6}$$

The kernel function maps low-dimensional data into high-dimensional space, and selecting an appropriate kernel function can significantly improve the model's ability to handle nonlinear problems. This paper uses the radial basis kernel function:

$$K(x_i, x) = \exp\left\{-\frac{|x - x_i|^2}{2\sigma^2}\right\} \tag{7}$$

In the equation, σ is the parameter of the kernel function. The radial basis kernel function uses the expression of $x - x_i$ for the input variables, which simplifies the processing and has good analytical properties. It is radially symmetric and smooth, making it suitable for small sample analysis.

By substituting the radial basis kernel function into Equation (7), the specific expression of the discriminant function can be obtained as follows:

$$f(x) = \mathrm{sgn}\left\{\sum_{i \in SV} \alpha_i y_i \exp\left(-\frac{|x - x_i|^2}{2\sigma^2}\right) + b\right\} \tag{8}$$

2.2. Confidence Level

The confidence level, also known as the level of confidence, refers to the degree to which an individual believes in the truthfulness of a proposition, i.e., the probability measure of the rationality of the degree of belief. The confidence level is also known as reliability or confidence coefficient.

The one-vs-one method is a solution for multiclass problems in the LS-SVM. It first constructs a classifier with two samples of different categories and then constructs a binary classifier for each class with respect to the other classes. When there are k classes to be classified, we obtain $k(k-1)/2$ sub-classifiers. During the classification stage, the samples

are input into all $k(k-1)/2$ sub-classifiers to obtain multiple classification results. Finally, the class with the most votes is selected as the output of the result.

The optimal classification hyperplane function of the LS-SVM mentioned earlier is as follows [24]:

$$h(x) = \mathrm{sgn}(y(x)) = \mathrm{sgn}(\sum_{i=1}^{n} \alpha_i K(x_i, x) + b) \tag{9}$$

Therefore, the distance from the test sample to the optimal classification hyperplane can be obtained as follows:

$$d(x_i) = \mathrm{sgn}(\omega x + b)/|\omega| \tag{10}$$

By substituting the kernel function, the distance equation can be transformed as follows:

$$d(x_i) = \mathrm{sgn}\left(\sum_{j=1}^{i} y_i \alpha_i K(x_j x_i + b)\right)/|\omega| \tag{11}$$

From the analysis of the principle of the LS-SVM, when the distance between the test sample and the optimal classification hyperplane is too close, $d(x_i)$ is smaller than the threshold for classification evaluation, the LS-SVM does not accept this classification result because the classification confidence level is too low. By analyzing the definition of confidence level, it can be known that in the model of the LS-SVM, the confidence level is proportional to the distance from the test sample to the optimal hyperplane, i.e., the larger the $d(x_i)$, the greater the confidence level of the classification result, and conversely, the smaller the $d(x_i)$, the lower the confidence level of the classification result. Therefore, the evaluation equation for confidence level can be defined as follows:

$$\lambda_j = \exp(-1/|d(x_i)|) \tag{12}$$

However, this confidence level only considers the distance from the test sample to the optimal classification hyperplane. When the test point is too far away from the optimal hyperplane, it may be an outlier, and the confidence level of the outlier is often very high. Therefore, to avoid interference from outliers, we introduce a variable p_i into the equation for the confidence level. The variable p_i is defined as the probability of the occurrence of training samples in the neighborhood about the test sample points with the same class as the classification result. The greater the consistency between the classification result of the test point and the classification results of the surrounding training samples, the greater the probability that the test point belongs to that class. Therefore, the improved equation for evaluating the confidence level is as follows:

$$\lambda_j = \exp(-1/|d(x_i)| * p_i) \tag{13}$$

In the equation, p_i is the probability of the occurrence of the training points of the same type as the test sample in the vicinity of the test sample:

$$p_i = j_s/j \tag{14}$$

In the equation, j represents the number of points in the neighborhood of the sample and j_b represents the number of points in the neighborhood that have the same classification result as the test point.

2.3. OLS-SVM

The OLS-SVM mainly involves modeling new data into the algorithm and then deleting some samples according to certain principles, ensuring the model's accuracy and saving computation time. Combining the principles of the LS-SVM algorithm and online learning in order to ensure the diversity and sparsity of the entire data structure, this paper mainly deletes data based on the LS-SVM block matrix inversion, which requires the use of the

Lagrange multiplier. When the absolute value of the Lagrange multiplier pair is the smallest, the contribution of this sample to the overall algorithm is the lowest. This algorithm is suitable for systems with small parameter fluctuations.

The time to solve the optimal classification hyperplane mainly involves computing H^{-1}. If the updated H^{-1} can be calculated through a recursive computation when adding or deleting samples, it can save a lot of time for the algorithm update.

1. Incremental learning

Assuming that the current LS-SVM model has learned l samples and the corresponding H_l^{-1} has been obtained, when a new sample (x_{l+1}, y_{l+1}) is added at this point:

$$H_{l+1} = \Omega_{l+1} + \gamma^{-1}E = \begin{bmatrix} H_l & V_{l+1} \\ V_{l+1}^T & v_{l+1} \end{bmatrix} \tag{15}$$

In the equation, $V_{l+1} = [k(x_{l+1}, x_1), \cdots, k(x_{l+1}, x_l)]^T$, $v_{l+1} = k(x_{l+1}, x_{l+1}) + 1/\gamma$. According to the property of the block matrix inversion, it can be obtained using:

$$H_{l+1}^{-1} = \begin{bmatrix} H_l & V_{l+1} \\ V_{l+1}^T & v_{l+1} \end{bmatrix}^{-1} = \begin{bmatrix} H_l^{-1} + H_l^{-1}V_{l+1}\rho^{-1}V_{l+1}^T H_l^{-1} & -H_l^{-1}V_{l+1}\rho^{-1} \\ \rho^{-1}V_{l+1}^T H_l^{-1} & \rho^{-1} \end{bmatrix} \tag{16}$$

In the equation, $\rho = v_{l+1} - V_{l+1}^T H_l^{-1} V_{l+1}$. Therefore, it is not necessary for the recalculation, and the computational cost is reduced by using a recursive approach.

2. Decremental learning

When a redundant sample needs to be removed after adding a new data point, a random sample can be removed, or the oldest data can be removed in chronological order. This approach has good performance for time-varying data models, but for static models, such removal can cause uneven data distribution and even lead to a decrease in model accuracy. Usually, the following three principles can be used to design decremental algorithms:

(1) Minimum classification error rate-driven strategy

Using the minimum error rate strategy means that when data is removed, the retained samples follow the minimum error rate feature samples. However, the classification error rate needs to be compared with the actual classification results after the model has obtained the learning results. When the data scale is large, this strategy often takes a long time.

(2) Maximum inter-class distance-driven strategy

Using the maximum inter-class distance-driven strategy means that when data is removed, the retained data follows the maximization of the distance between the data classes, ensuring no clustering phenomenon in the data within a certain range and ensuring that the data distribution is uniform. This strategy ensures that the data distribution is uniform and does not ignore other possibilities due to the density of a certain class of data. However, the increase in inter-class distance makes data not prioritize accuracy, and such decremental algorithms often do not improve the model accuracy.

(3) Hybrid-driven strategy

Based on the considerations of the above two strategies, a hybrid-driven strategy is proposed in this paper, which means that in the process of each decremental calculation, the retained data needs to ensure the expansion of the interval while ensuring the minimum error rate. This can ensure that the retained data is evenly distributed while improving the model's accuracy.

In summary, the steps for establishing an online LS-SVM model are as follows:

Step 1: Extracting and establishing a training sample set based on experimental data.

Step 2: Normalizing the input samples and establishing the LS-SVM model.

Step 3: When new data is added, updating the data matrix and performing incremental learning.

Step 4: Obtaining the new LS-SVM model training results.

Step 5: Performing the decremental learning based on the hybrid-driven approach according to the new training results.

Step 6: Waiting for new data to enter and return to Step 3.

3. Fault Analysis of Lithium-Ion Batteries

After analyzing the types of faults that occur in the actual application of lithium-ion batteries, some battery problems, such as high battery temperature, can be directly determined by obtaining temperature data through automotive sensors. However, the effects of battery aging, overcharging, and over-discharging are gradual and cannot be directly determined through external battery data collected by sensors. The occurrence of these types of faults often leads to irreversible chemical reactions inside the battery. Therefore, this section designs corresponding charge and discharge experiments for overcharging, over-discharging, and aging issues. Based on the experimental results, the regularities of overcharging, over-discharging, and aging issues were identified, the causes of faults were analyzed, and characteristic fault data were extracted to prepare for the establishment of a fault diagnosis model in the future.

3.1. Charging and Discharging Characteristics of Lithium-Ion Batteries

In practical use, the discharge mode of a lithium-ion battery changes with the changing operating conditions. However, the charging mode of a lithium-ion battery is generally charged using a CC-CV (constant current-constant voltage) method. First, the battery was charged with a constant current until it reached the standard voltage, and then it was charged with a constant voltage until the charging current was reached. The voltage and current curves of the standard charging process for lithium-ion batteries at 25 °C are shown in Figure 1. From the figure, it can be seen that at the beginning of constant current charging, the voltage quickly rose and then entered the charging voltage plateau for constant voltage charging, and the current gradually decreased until 0.2C. At this point, if the battery continues to be charged, it might cause overcharging of the battery, which could lead to a decrease in overall battery performance and even cause accidents.

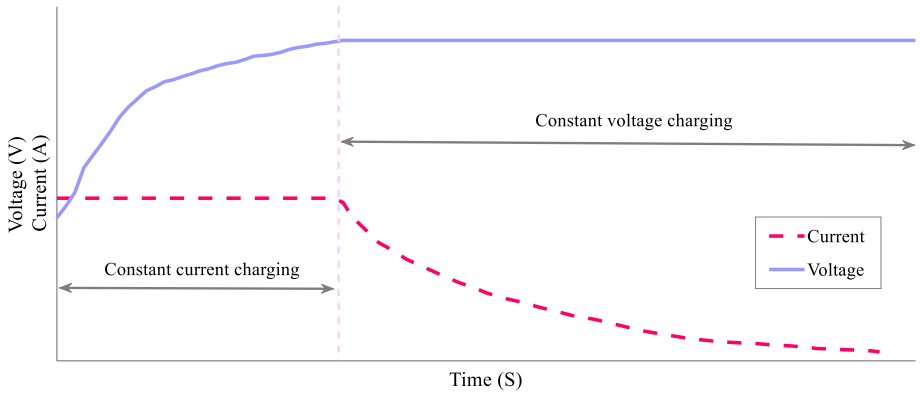


Figure 1. Lithium-ion battery charging voltage and current curve.

Over-discharging refers to the situation where a battery is discharged beyond its cutoff voltage, causing internal damage to the battery's chemical structure and resulting in irreversible harm to the battery. During the discharge process of a lithium-ion battery, a good discharge voltage curve can be obtained at a fixed discharge rate. The performance of the battery is affected differently at different discharge rates. Figure 2 shows the discharge characteristic curve of a lithium-ion battery at different discharge rates and constant current at the same temperature. It is evident from the figure that even at the same capacity, the discharge capability of the battery varied with different discharge rates. The higher the discharge rate, the lower the voltage at which the battery entered the voltage plateau and the shorter the time spent on the discharge plateau. Large discharge rates caused rapid

internal reactions and polarization of the battery, resulting in an increase in the battery's polarization internal resistance, which prevented the battery from fully discharging. In practical applications of lithium-ion batteries in automobiles, sudden acceleration and deceleration often result in large discharge rates of the power battery. Long-term large discharge rates can cause permanent and irreversible damage to the battery.

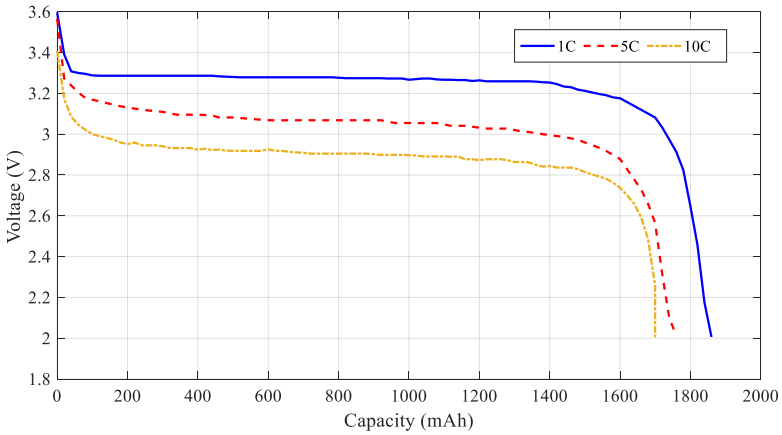


Figure 2. The charge and discharge curve of different rates.

3.2. Analysis of Battery Aging Faults

As a complex chemical reaction system, lithium-ion batteries undergo irreversible chemical reactions during use, resulting in different external output states as the accumulation of irreversible reaction products gradually increases. This irreversible reaction is manifested as battery aging.

Battery aging is one type of battery failure and can be accelerated by abnormal use of lithium-ion batteries, such as deep discharge and over-current output, inappropriate external temperatures, and other factors. The internal changes of the battery during the aging process mainly include the degradation of active materials inside the battery, the aging and deterioration of some conductive agents and other chemical substances on the electrodes, the formation of a membrane on the electrolyte that prevents the passage of lithium ions, and the corrosion and deterioration of the metal on the exposed battery electrode surface. The microscopic changes inside the battery often result in changes in some performance parameters of the lithium-ion battery at a macroscopic level.

To research the external manifestations of the internal aging process of batteries, this article designs a fast cycle charge and discharge experiment on batteries to obtain battery aging data. The Arbin BT-ML-30 V/10 A power battery tester produced by Arbin in the United States was used as the battery data acquisition platform. This power battery tester is suitable for various battery performance tests, with a voltage measurement range of 0–30 V, a current measurement range of 0–10 A, a voltage accuracy of up to 0.1 mV, and a current accuracy of up to 0.1 mA. The specific experimental platform and sample battery are shown in Figure 3.

The experimental study employed a cohort of 600, which 2400 mAh 18,650 batteries as the research subjects. According to the product specification, the charging cutoff voltage of the battery is 3.7 V, the discharge cutoff voltage is 3.2 V, and the maximum discharge current is 5 A. Considering that the number of battery cycles is the most significant factor affecting battery aging, this experiment conducted aging experiments on new batteries to quickly obtain aging data. The battery was charged at 3C, and when it was fully charged after 20 min, it was discharged at 3C for another 20 min. The voltage data of nearly 2000 cycles of the battery are shown in Figure 4.



Figure 3. Sample battery and battery experiment platform.

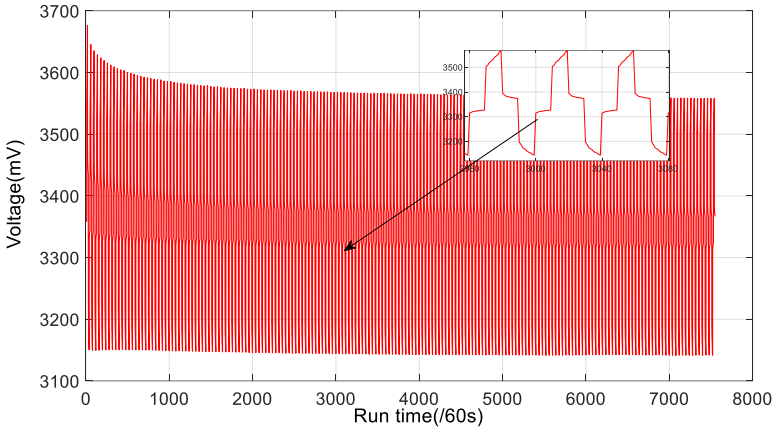


Figure 4. Cyclic charge–discharge voltage recording cure.

From the figure, under the same current and charging power, the highest voltage of the battery continuously decreased with the increase in the number of cycles. This proves that as the battery ages, its energy conversion capacity decreases, and charging the battery becomes more difficult under the same power. This battery's standard charging cutoff voltage is 3.7 V. Assuming that the battery is a standard battery when not in use, the battery voltage can reach about 3.7 V in the first few cycles, and the actual capacity charged should be close to the rated capacity. When the battery was cycled 50 times, the highest voltage under the same power charging was less than 3.6 V and gradually decreased with the increase in the number of cycles. At this time, the battery's charging capacity greatly decreased, proving that as the degree of battery aging became more severe, the battery's charging capacity decreased.

The decrease in charging voltage under the same current is potentially due to an increase in internal resistance caused by battery cycling, according to Ohm's law. The increase in internal resistance during battery charging can cause the battery temperature to rise, which will accelerate the battery's aging, forming negative feedback. To verify the correlation between the degree of battery aging and the internal resistance of the battery, five batteries of the same model were selected for cycle charge and discharge tests, and the internal resistance of each battery after every 100 cycles was recorded and plotted as shown in Figure 5.

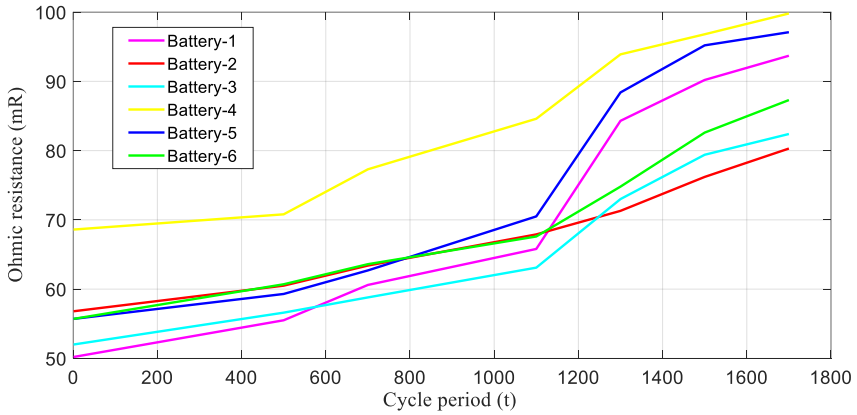


Figure 5. Cyclic charge–discharge battery resistance recording cure.

Overall, with the increase in battery cycling cycles, the internal resistance of the battery showed an increasing trend. From the figure, the increase in the internal resistance of the battery was not significant before the battery was cycled for 1000 cycles, but after more than 1000 cycles, the internal resistance of the battery showed a rapid increase. At this time, the negative feedback of resistance and temperature on the degree of aging became larger, leading to a rapid increase in the battery's internal resistance.

Based on the descriptions of the two experiments above, different degrees of battery aging affect the changes in the battery's charging voltage and internal resistance, and the decrease in charging voltage often represents the attenuation of the battery capacity. Therefore, the battery's capacity and internal resistance are positively correlated with the degree of battery aging. Therefore, these two indicators can be used to measure the degree of battery aging, as shown in Figure 6.

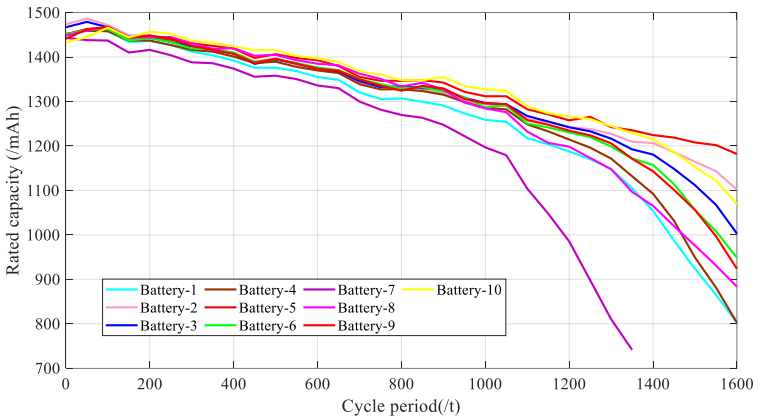


Figure 6. Cyclic charge–discharge battery capacity recording curve.

3.3. Battery Overcharging Fault Analysis

In general, overcharging of lithium-ion batteries refers to the battery being charged even after reaching full capacity. During the charging process, the battery cell is protected by a cutoff current. However, in engineering applications, batteries are often charged and discharged as a whole battery pack. Due to the inconsistency of cells in the battery pack and the improper design of battery management systems (BMS), overcharging of the battery still occurs. Charging a battery is a process of converting electrical energy into chemical energy, which often generates heat during the charging process. Therefore, overcharging is an important type of battery failure, and thermal runaway often occurs during the charging stage of many battery systems.

Under normal circumstances, lithium in the battery exists in the form of ions. However, during overcharging, some lithium ions on the negative electrode surface are reduced to

lithium metal, which then forms dendrites. As the lithium dendrites continue to grow, the separator between the electrolyte and electrodes is punctured, causing an internal short circuit between the positive and negative electrodes. After a short circuit occurs in a lithium-ion battery, the short-circuit current causes the internal temperature to rise sharply, and high temperature induces a series of side reactions, mainly including the decomposition of the solid electrolyte interface (SEI) film, the reaction between the positive and negative electrodes and the electrolyte, and the decomposition of the electrolyte. Therefore, research on battery overcharging mainly focuses on the effect of multiple overcharging on the battery surface temperature. The battery was constantly overcharged with a constant current until it failed, and the changes in battery voltage and surface temperature were recorded, as shown in Figure 7.

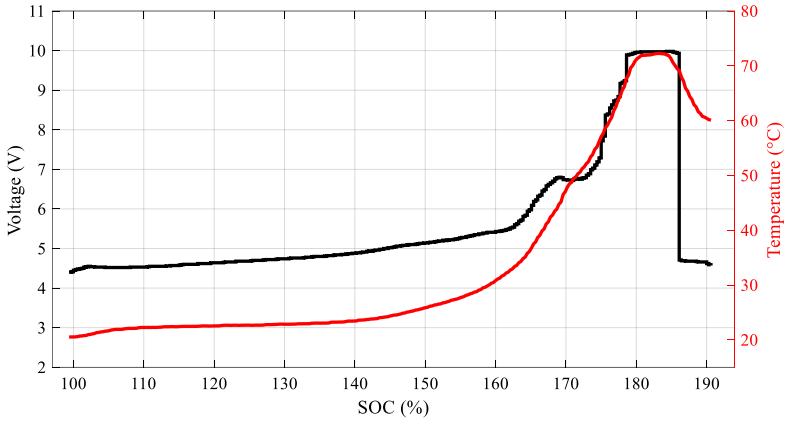


Figure 7. Voltage and temperature curve during overcharging.

According to the results of the constant current overcharging experiment, it can be observed that the battery's temperature increased continuously after overcharging. When the battery was first overcharged, the surface temperature of the battery increased rapidly. When the overcharging exceeded 60%, the temperature and voltage of the battery increased rapidly. At this point, the battery had reached the limit of thermal runaway, and further charging caused the temperature of the battery to become too high, leading to failure after overcharging by 80%. This demonstrates that overcharging has a significant correlation with the temperature of the battery. However, in practical battery applications, it is challenging for the battery to reach an overcharge of 60%. Typically, charging up to 110% of the battery capacity is more common. Therefore, a new battery was selected for the experiment, and it was overcharged multiple times with 110% capacity to observe the changes in the battery's surface temperature during multiple small overcharging events. The experimental results are shown in Figure 8.

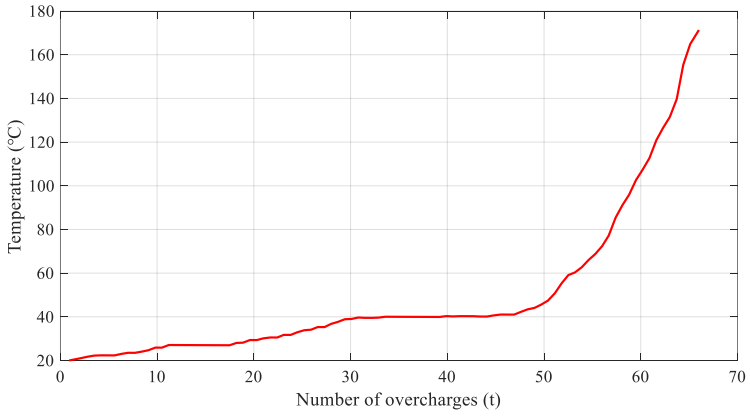


Figure 8. Temperature curve in the overcharging experiment.

In the experiment of multiple overcharging with 110% capacity, the battery's heat generation was not significant when it was first overcharged. However, with the increasing number of overcharging cycles, the accumulation of lithium dendrites inside the battery caused a rapid increase in heat generation after overcharging for 50 cycles. After 60 cycles, the highest surface temperature of the battery had exceeded 100 °C, and further overcharging caused the temperature to rise rapidly. It can be seen that the battery's performance deteriorates rapidly after multiple overcharging events, generating a significant amount of heat, which poses a significant safety hazard to the battery's surrounding system and operators.

Based on the above two experiments, we can see that the overcharging fault of the battery is related to the battery's performance and system safety level. The main external manifestation of the overcharging fault is the temperature rise, and with the gradual increase in the degree of overcharging, the surface temperature of the battery rises rapidly. Therefore, the highest surface temperature during battery charging can be used as a measure of the degree of overcharging.

3.4. Battery Over-Discharge Fault Analysis

Compared to the charging process, the discharge process of a battery is an endothermic reaction and generally does not lead to a thermal runaway event. However, over-discharging has a more significant impact on the battery's overall performance. When the battery is over-discharged, irreversible damage is caused to the negative electrode plate and its SEI surface film, affecting the lithium-ion insertion resistance during its subsequent recharge. This makes the charging process difficult, and irreversible loss of the negative electrode active material can cause premature battery failure. In practical applications, most batteries are still used in the discharge phase. Therefore, it is essential to study the over-discharge fault of the battery.

The battery's discharge process is mainly related to the discharge rate and depth of discharge (DOD). Therefore, the main focus is on studying the effects of different discharge rates and depths of discharge on the battery's performance. As shown in Figures 2–4, the higher the discharge rate, the less energy the battery can release, and the lower the voltage plateau. To better study the effect of DOD on lithium batteries, this paper selected multiple groups of batteries for different DOD experiments at a C/2 discharge rate. The batteries were divided into two groups, and after the battery was fully charged, it was discharged to 2.7 V and 2 V, respectively. The voltage curve after discharging to different depths once and 100 times was compared, as shown in Figures 9 and 10.

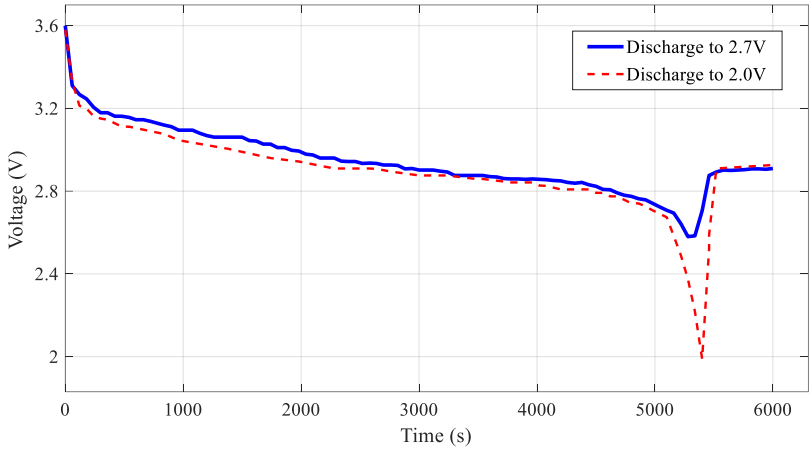


Figure 9. The voltage curve of the first deep discharge.

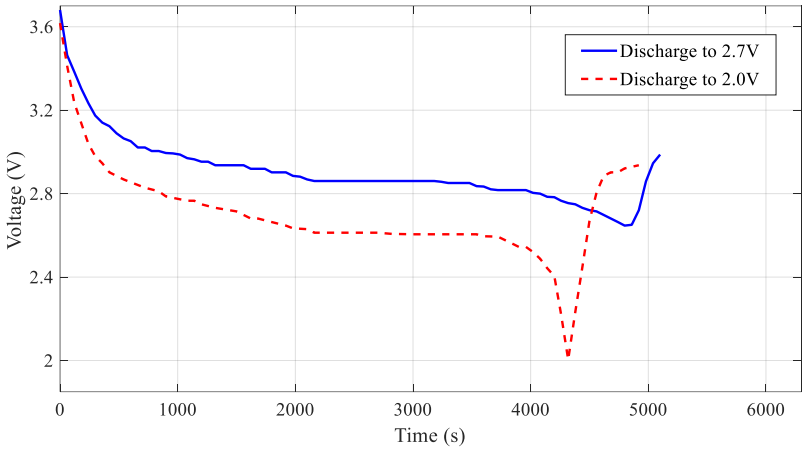


Figure 10. The voltage curve of the one-hundredth deep discharge.

By comparing the above figures, it can be seen that in the first over-discharge experiment, the battery's discharge voltage was almost the same. However, after 100 cycles of over-discharging, the overall discharge voltage of the battery decreased, and the discharge time became shorter. The longer the time spent on the voltage plateau, the faster the performance of the battery that is discharged to 2 V deteriorates compared to the battery discharged to 2.7 V. Therefore, the voltage plateau during battery discharge can be used as a measure of the degree of over-discharge.

In summary, in the use of lithium-ion batteries, the aging of the battery and faults caused by overcharging and over-discharging have different effects on the external parameters of the battery. These faults do not occur suddenly but gradually change as the battery is used. When the battery identifies them as faults, irreversible damage has already occurred inside the battery. Multiple cycle experiments have confirmed that although these faults often affect the battery's performance for a long time, the damage is irreversible. Therefore, after in-depth research on the parameter changes caused by the three types of faults, the data that best reflects the fault was selected as the dataset for the fault diagnosis model.

4. Results

Based on the analysis in the previous section, the external parameters of batteries related to aging, overcharging, and over-discharging faults are related to the battery's capacity, internal resistance, surface temperature, and discharge voltage. Therefore, 500 sets of data were extracted for batteries with aging, overcharging, over-discharging, and normal conditions, respectively, resulting in a total of 2000 sets of data as the training set. After completing the collection of lithium-ion battery data, the sampled data set $\{(x_i, y_i), i = 1, 2, \ldots, n\}$ consisted of $x_i \in R^4$, which is composed of charging voltage, internal resistance, and surface temperature. y_i represents the actual fault type of the battery. The types of the three faults and normal data are respectively labeled as 1 to 4 and brought into y_i. The training samples for the fault diagnosis model were obtained, and the specific data information is shown in Table 1.

Table 1. Training sample of battery fault diagnosis model.

Sample Count	Battery Capacity (mAh)	Battery Internal Resistance (mΩ)	Battery Surface Temperature (°C)	Battery Discharge Voltage (V)	Fault Type
1	2134	79	19.7	3.2327	Aging
2	2243	52	37.3	3.2674	Overcharging
3	2357	51	20.4	3.3657	Normal
...	...	...	...	...	...
2000	2198	47	22.3	3.1692	Over-discharging

The calculation of the LS-SVM was performed, and the initial parameters were continuously adjusted to achieve the optimal diagnostic effect of the model. Due to the different dimensions and rates of change of voltage, temperature, and other parameters, the training sample data were standardized using the Z-score method to avoid affecting the accuracy and generalization ability of the LS-SVM. The standardized data not only had the same dimension but also followed a normal distribution, which performed well in representing inter-class distances and speeding up the calculation of confidence intervals. The equation for the Z-score standardization is as follows:

$$x^* = \frac{x - u}{\sigma} \tag{17}$$

Among them, x^* is the standardized data, μ is the mean of this type of sample, and σ is the standard deviation of the sample.

After obtaining the normalized training samples, the sample dataset was divided into 10 subsets on average, and one subset was taken as the test set, while the other subsets were used as the training set. The LS-SVM model was trained, and the accuracy of the LS-SVM model was calculated and saved. The above process was repeated so that each subset became a trained set. After training, we selected the model with the highest accuracy as the fault diagnosis model and judged the new data after it entered the model. Figures 11 and 12 show the model accuracy of the SVM and LS-SVM trained ten times on fault data, respectively.

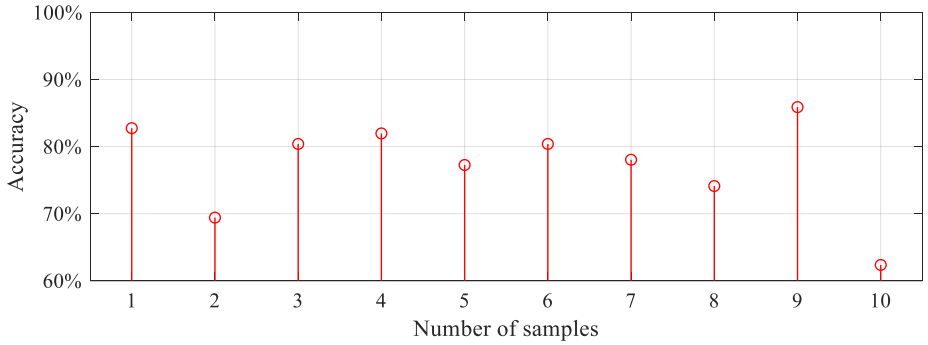


Figure 11. The model accuracy of the SVM trained 10 times.

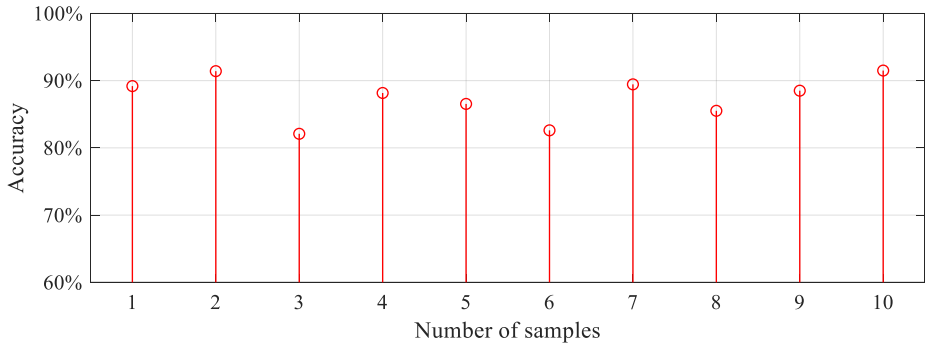


Figure 12. The model accuracy of the LS-SVM trained 10 times.

Through vertical comparison, it is not difficult to see that the LS-SVM model had a generally high accuracy compared to the SVM model. At the same time, the LS-SVM model had consistently maintained an accuracy of over 80% over 10 training sessions, with the highest accuracy reaching 92.5%. This indicates that the minimum quadratic SVM was superior to ordinary SVM models in terms of generalization ability and accuracy in judging fault data.

When new data enters the model, the LS-SVM model makes a fault-type judgment and provides confidence levels for each judgment. The confidence level represents the probability of the fault occurring, and the addition of confidence level solves the disadvantage of an LS-SVM that can only make a right or wrong judgment, making the judgment of the battery fault-type clearer, introducing 1500 cycles of aging battery data into the LS-SVM fault diagnosis model, and obtaining the confidence level, as shown in Figure 13.

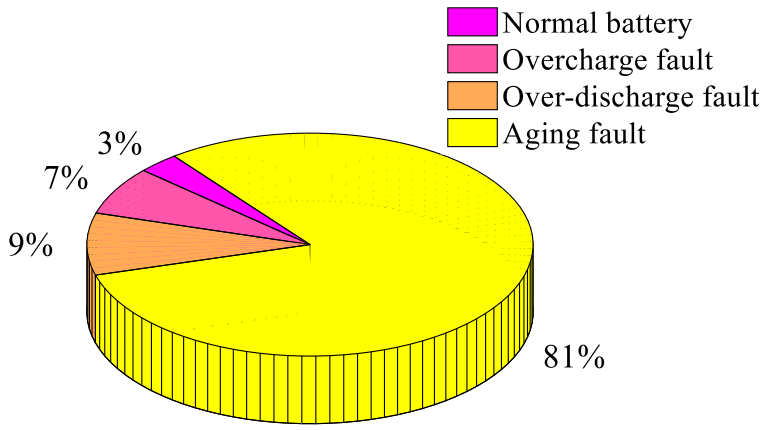


Figure 13. Confidence statistical chart.

From the above figure, it can be seen that the LS-SVM model had a confidence level of 82% in the aging data. Therefore, this data was classified as a battery aging fault type. In practical applications, when more than three sets of fault data were collected, the model's judgment was trusted, the average of the three confidence levels was brought into the FMEA fault model, and the calculation results were fed back to the battery BMS system.

In order to verify the confidence level and the performance of the least squares support vectors in fault diagnosis, a comparison was made with the naive Bayesian fault diagnosis model used in the references [25,26]. The study selected 100 sets of aging fault chapter battery data and 100 sets of normal battery data to test the naive Bayesian model, SVM surface model, and LS-SVM model, and obtained the fault judgment confidence results of the three models, as shown in Figures 14 and 15.

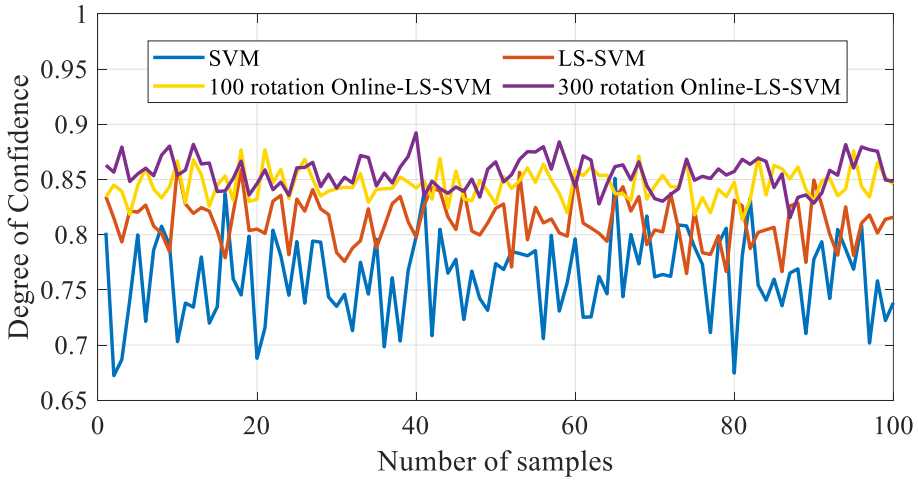


Figure 14. Aging fault confidence comparison.

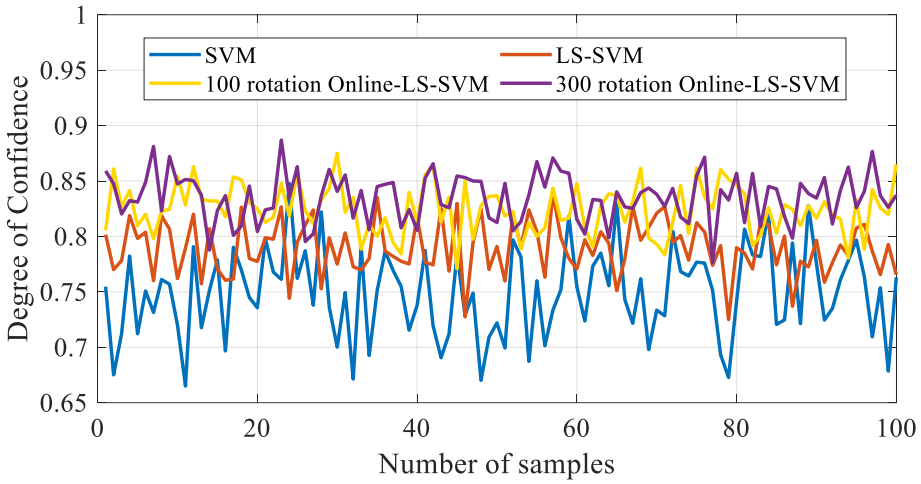


Figure 15. Normal battery confidence comparison.

From the comparison results, it can be observed that the blue line represents the confidence level of the LS-SVM. It can be clearly seen that the confidence level of the LS-SVM was high for both fault data and normal battery data. At the same time, the fluctuation amplitude of the LS-SVM was the smallest, proving that it was more accurate in judging fault data, had a small overall confidence entropy value, and had a stable diagnostic level. The problem of battery failure had a gradual nature. Taking battery aging as an example, the data of battery aging failure appeared when the battery was cycled 200 times. However, compared to the cycle life of lithium batteries from 1500 to 2000 cycles, cycling 200 weeks was not considered an aging failure. Taking data from 100 batteries cycled 200 times and bringing it into the three models, the confidence levels of the three models are shown in Figure 16.

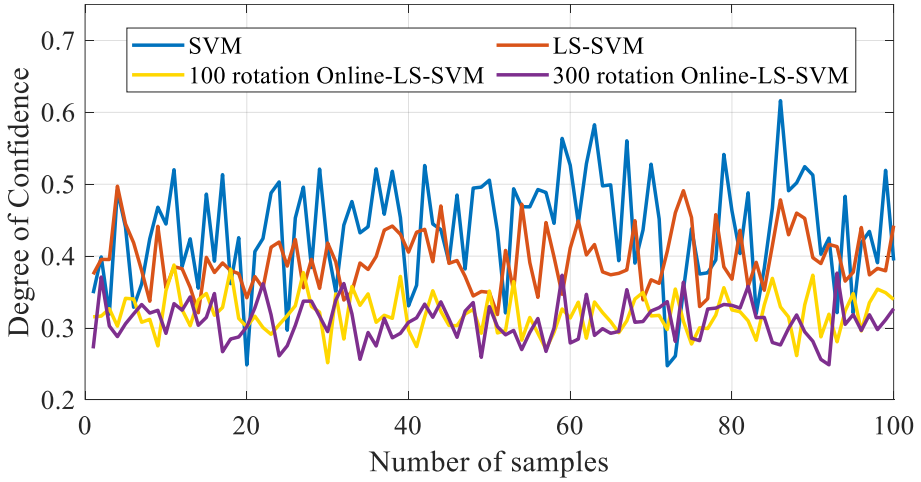


Figure 16. The cycle of 200 times battery confidence comparison.

From the comparison of the confidence levels of various data in the above figure, it can be seen that for batteries with fault symptoms, the LS-SVM did not provide more than 50% of the judgment. On the contrary, both naive Bayesian and SVM algorithms provided more than 50% of the judgment, which could cause incorrect fault alarms in practical applications. When the fault data was input into the LS-SVM fault diagnosis model, the model provided judgments with high confidence, avoiding the occurrence of misdiagnosis. At the same time, the battery fault diagnosis model did not only provide 100% judgment but also provided confidence levels for each fault type, which could reflect the relationship and changes between battery faults to a certain extent.

5. Conclusions

This study introduced a battery fault diagnosis model utilizing an OLS-SVM tailored for lithium-ion battery faults. Selected for its capability to process small, continuously nonlinear battery data, the OLS-SVM algorithm was employed. Experimental analysis facilitated the extraction of distinct fault feature data from various battery malfunctions. Utilizing this data, a diagnostic model was constructed, integrating confidence intervals to estimate fault likelihood. Subsequent applications of this trained model demonstrated its proficiency in fault detection. Empirical results confirm the OLS-SVM's efficiency in swift fault categorization and highlight the added benefit of confidence intervals in addressing the intricacies of gradual battery faults. Comparative analysis with both the SVM and LS-SVM methods further underscored the OLS-SVM's superior accuracy in diagnosing static fault data.

Author Contributions: Methodology, T.Z.; Resources, R.L.; Writing—original draft, T.Z.; Writing—review & editing, Y.Z. All authors have read and agreed to the published version of the manuscript.

Funding: This research received no external funding.

Data Availability Statement: The data presented in this study are available on request from the corresponding author. The data are not publicly available due to the data in the paper has a certain degree of confidentiality.

Conflicts of Interest: The authors declare no conflict of interest.

References

1. Ramdon, S.K. *Nanoscale Characterization of Aged Li-Ion Battery Cathodes*; The Ohio State University: Columbus, OH, USA, 2013.
2. Liu, J.; Wang, Z.; Bai, J.; Gao, T.; Mao, N. Heat generation and thermal runaway mechanisms induced by overcharging of aged lithium-ion battery. *Appl. Therm. Eng. Des. Process. Equip. Econ.* **2022**, *212*, 118565. [CrossRef]
3. Tan, M.; Liu, W.-D.; Shi, X.-L.; Sun, Q.; Chen, Z.-G. Minimization of the electrical contact resistance in thin-film thermoelectric device. *Appl. Phys. Rev.* **2023**, *10*, 021404. [CrossRef]
4. Feng, X.; Pan, Y.; He, X.; Wang, L.; Ouyang, M. The internal short circuit in large-format lithium-ion battery using model-based fault-diagnosis algorithm. *J. Energy Storage* **2018**, *18*, 26–39. [CrossRef]
5. Zhao, Y.; Liu, P.; Wang, Z. Electric vehicle battery fault diagnosis based on statistical method. *Energy Procedia* **2017**, *105*, 2366–2371. [CrossRef]
6. Lin, T.; Chen, Z.; Zhou, S. Voltage-correlation based multi-fault diagnosis of lithium-ion battery packs considering inconsistency. *J. Clean. Prod.* **2022**, *336*, 130358. [CrossRef]
7. Wu, L.; Liu, K.; Liu, J.; Pang, H. Evaluating the heat generation characteristics of cylindrical lithium-ion battery considering the discharge rates and N/P ratio. *J. Energy Storage* **2023**, *64*, 107182. [CrossRef]
8. Zhou, S.; Chen, Z.; Lin, T. Lithium-Ion Battery Cell Open Circuit Fault Diagnostics: Methods, Analysis, and Comparison. *IEEE Trans. Power Electron.* **2022**, *38*, 2493–2505. [CrossRef]
9. Zhang, S.; Jiang, S.; Wang, H.; Zhang, X. A novel dual time-scale voltage sensor fault detection and isolation method for series-connected lithium-ion battery pack. *Appl. Energy* **2022**, *322*, 119541. [CrossRef]
10. Wang, Y.; Meng, D.; Wang, Y.; Li, R.; Zhou, Y. Research on health state estimation methods of lithium-ion battery for small sample data. *Energy Rep.* **2022**, *8*, 2686–2698. [CrossRef]
11. Tang, A.; Jiang, Y.; Yu, Q.; Zhang, Z. A hybrid neural network model with attention mechanism for state of health estimation of lithium-ion batteries. *J. Energy Storage* **2023**, *68*, 107734. [CrossRef]
12. Yu, Q.; Nie, Y.; Liu, S.; Li, J.; Tang, A. State of health estimation method for lithium-ion batteries based on multiple dynamic operating conditions. *J. Power Source* **2023**, *582*, 233541. [CrossRef]
13. Wang, Y.; Meng, D.; Chang, Y.; Zhou, Y.; Li, R.; Zhang, X. Research on online parameter identification and SOC estimation methods of lithium-ion battery model based on a robustness analysis. *Int. J. Energy Res.* **2021**, *45*, 21234–21253. [CrossRef]
14. Yang, Y.; Zhao, L.; Yu, Q.; Liu, S.; Zhou, G.; Shen, W. State of charge estimation for lithium-ion batteries based on cross-domain transfer learning with a feedback mechanism. *J. Energy Storage* **2023**, *70*, 108037. [CrossRef]
15. Chen, W.; Cai, Y.; Li, A.; Su, Y.; Jiang, K. Remaining Useful Life Prediction for Lithium-Ion Batteries Based on Empirical Model and Improved Least Squares Support Vector Machine. In Proceedings of the Chinese Intelligent Automation Conference, Zhanjiang, China, 5–7 November 2021. [CrossRef]
16. Zhang, D.-W.; Duan, Z.-M.; Li, P.; Zhang, X.-H. Simulation Research on Optimized Genetic LSSVM Used in Fault Diagnosis. *Comput. Simul.* **2010**, *27*, 164–167.
17. Wei, M.; Ye, M.; Li, J.B.; Wang, Q.; Xu, X.X. State of charge estimation for lithium-ion batteries using dynamic neural network based on sine cosine algorithm. *Proc. Inst. Mech. Eng. Part D J. Automob. Eng.* **2022**, *236*, 241–252. [CrossRef]

18. Li, J.; Hu, Y.; Gao, J.; Zeng, L.; Zheng, Y.; Dai, W. Health state estimation of lithium-ion batteries based on GWO-LSSVM. *J. Underw. Unmanned Syst.* **2022**, *30*, 9. [CrossRef]
19. Zhang, Q.; Zha, X.; Wu, J.; Zhang, L.; Dai, W.; Ren, G.; Li, S.; Ji, N.; Zhu, X.; Tian, F. PSO-LSSVM-based Online SOC Estimation for Simulation Substation Battery. *Struct. Durab. Health Monit.* **2022**, *16*, 37–51. [CrossRef]
20. Adaikkappan, M.; Sathiyamoorthy, N. Modeling, state of charge estimation, and charging of lithium-ion battery in electric vehicle: A review. *Int. J. Energy Res.* **2022**, *46*, 2141–2165. [CrossRef]
21. Wang, Y.; Meng, D.; Li, R.; Zhou, Y.; Zhang, X. Research on interactive multi-model fault diagnosis method of Li-ion battery based on noise suppression. *Int. J. Energy Res.* **2021**, *45*, 13198–13218. [CrossRef]
22. Yibin, T.; Shi, Y.; Xin, Z.; Guanjun, L.; Zhong, L. A Novel Fault Diagnosis Strategy of MMC Battery Energy Storage System Based on SPVD. *J. Phys. Conf. Ser.* **2021**, *1754*, 012014. [CrossRef]
23. Jiang, L.; Deng, Z.; Tang, X.; Hu, L.; Lin, X.; Hu, X. Data-Driven Fault Diagnosis and Thermal Runaway Warning for Battery Packs Using Real-World Vehicle Data. *Energy* **2021**, *234*, 121266. [CrossRef]
24. Wang, Y.; Jiang, C. Fuzzy neural network expert system for fault diagnosis in power lithium battery application. *Electr. Meas. Instrum.* **2015**, *52*, 118–123.
25. Chen, Z.; Xiong, R.; Tian, J.; Shang, X.; Lu, J. Model-based fault diagnosis approach on external short circuit of lithium-ion battery used in electric vehicles. *Appl. Energy* **2016**, *184*, 365–374. [CrossRef]
26. Zhao, Y.; Liu, P.; Wang, Z.; Zhang, L.; Hong, J. Fault and defect diagnosis of battery for electric vehicles based on big data analysis methods—ScienceDirect. *Appl. Energy* **2017**, *207*, 354–362. [CrossRef]

Disclaimer/Publisher's Note: The statements, opinions and data contained in all publications are solely those of the individual author(s) and contributor(s) and not of MDPI and/or the editor(s). MDPI and/or the editor(s) disclaim responsibility for any injury to people or property resulting from any ideas, methods, instructions or products referred to in the content.